

Supporting Information

“Ion conductivity of acceptor doped sodium bismuth titanate: Influence of dopants, phase transitions and defect associates”

Leonie Koch,^{*,†,¶} Sebastian Steiner,^{*,‡,¶} Kai-Christian Meyer,[†] In-Tae Seo,[‡] Karsten Albe,[†] and Till Frömling[‡]

[†] *Fachgebiet Materialmodellierung, Institut für Materialwissenschaft, TU Darmstadt, Jovanka-Bontschits-Straße 2, D-64287 Darmstadt, Germany*

[‡] *Fachgebiet Nichtmetallisch-Anorganische Werkstoffe, Institut für Materialwissenschaft, TU Darmstadt, Alarich-Weiss-Straße 2, D-64287 Darmstadt, Germany*

[¶] *Contributed equally to this work*

E-Mail: koch@mm.tu-darmstadt.de; steiner@ceramics.tu-darmstadt.de

Density:

The density of the sintered pellets were investigated with the help of the Archimedes density method.

Table S 1: Fraction of the theoretical density of the processed compositions compared to the value of pure $\text{Na}_{0.5}\text{Bi}_{0.5}\text{TiO}_3$

Composition	Density (average over four samples) [g/cm ³]	Theoretical density compared to pure NBT [%]
NBT	5.84	97.95
0.1% Mg-NBT	5.81	96.88
0.2% Mg-NBT	5.62	93.64
0.5% Mg-NBT	5.79	96.53
1.0% Mg-NBT	5.80	97.36
1.5% Mg-NBT	5.77	96.25
2.0% Fe-NBT	5.78	96.48
4.0% Fe-NBT	5.81	96.77

As can be seen in Table S 1, the density of the Mg-doped NBT samples is slightly lower compared to the pure NBT and Fe-doped NBT samples. Nevertheless, the values always reach almost 95% of the theoretical density and higher. Hence, the sintering always leads to a sufficiently dense material with closed porosity.

Phase purity analysis by X-Ray Diffraction (XRD):

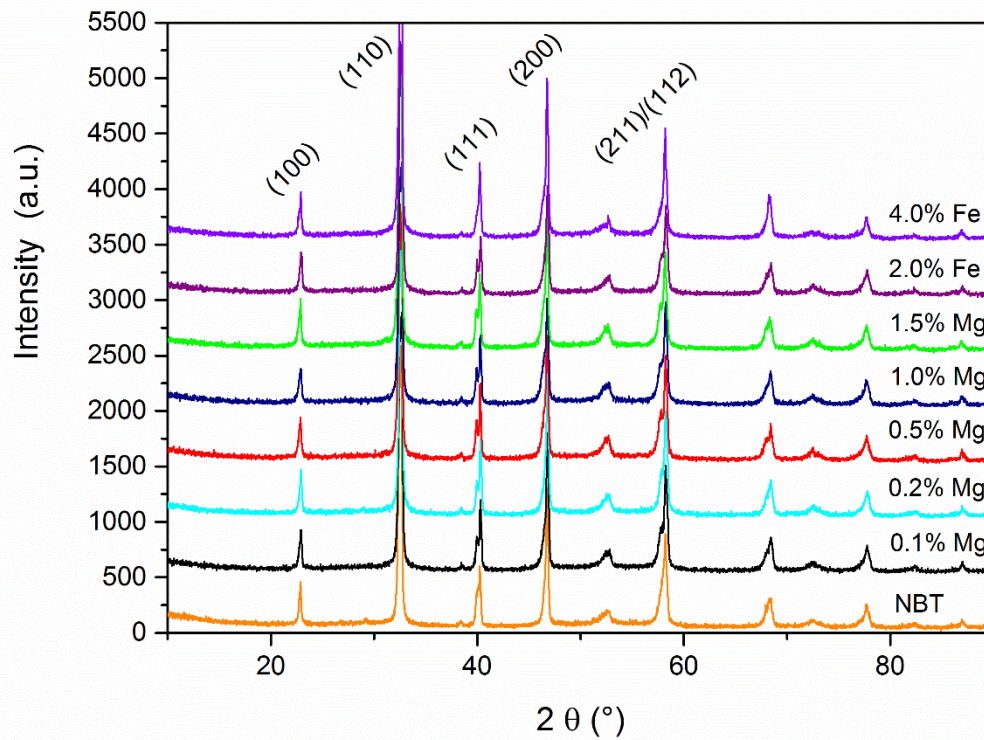


Figure S 1: XRD patterns of Mg-doped and Fe-doped as well as pure NBT

The processed compositions have been double calcined at 800°C and 850°C to avoid the occurrence of secondary phases. To prove the success of the processing Figure S1 depicts the XRD patterns of pure and Mg-doped NBT. The (200) peak shows no peak splitting which can be related to a pseudo cubic or rhombohedral structure. The (111) peak reveals a shoulder, which is indicative for a rhombohedral structure at room temperature^{1, 2}. The XRD results do not show any evidence of secondary phases even at high Mg-doping contents within the resolution of the used device.

Phase purity by Scanning Electron Microscopy (SEM) and Energy Dispersive X-Ray Spectroscopy (EDX):

The expected amount of secondary phases is lower than the sensitivity limit of the XRD method. According to this, SEM pictures were taken of the Mg-doped compositions to check for lower amounts of secondary phases. All pictures were taken on carbon sputtered samples in the back scattering electron (BSE) mode. Additionally, EDX was used to investigate the occurring secondary phases and the matrix.

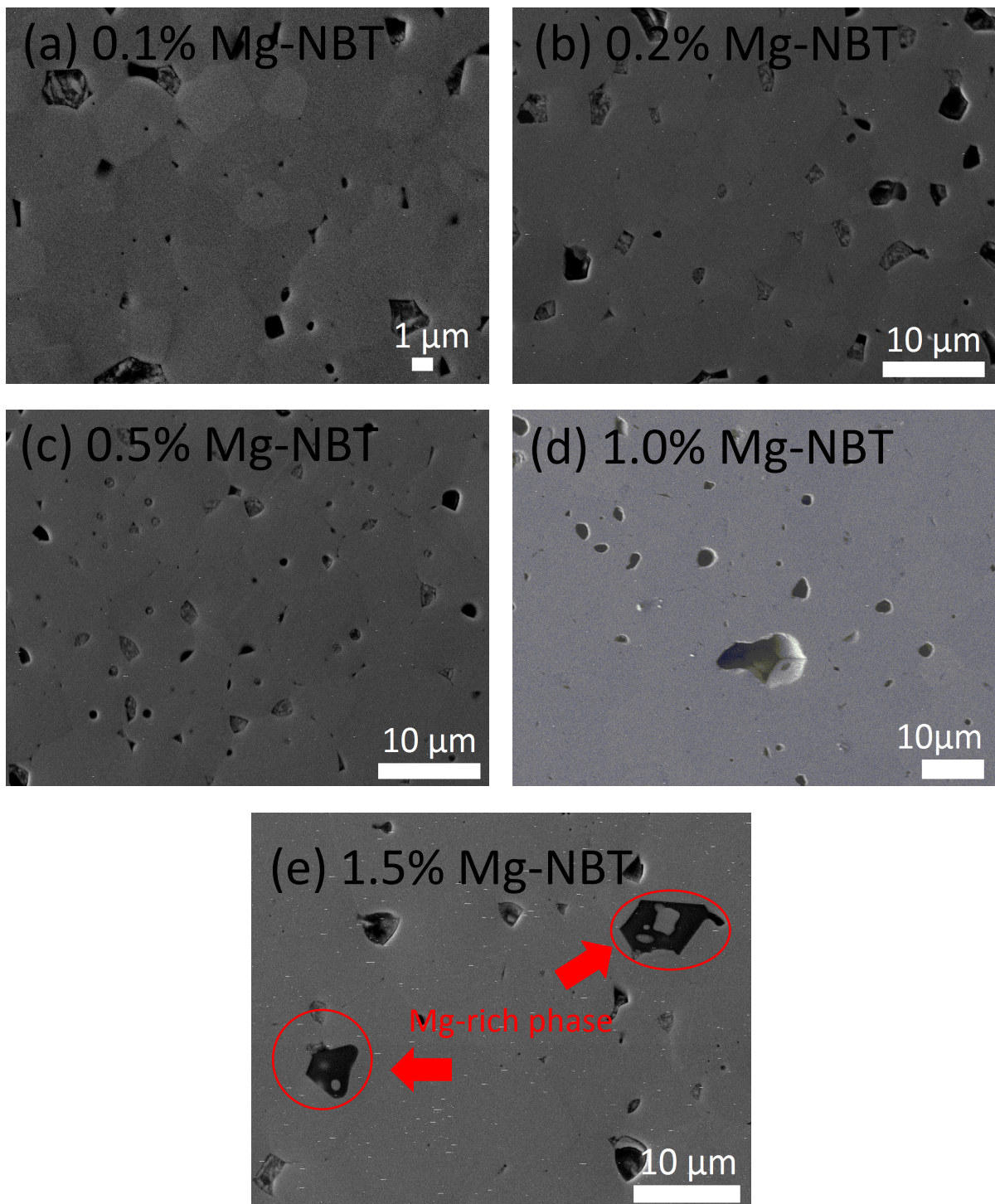


Figure S 2: SEM pictures of 0.1, 0.2, 0.5, 1.0 and 1.5 mol% Mg-doped NBT in BSE mode

No secondary phases were observed for all processed compositions by XRD. Additionally, no secondary phases have been detected in 0.1 (a), 0.2 (b), 0.5 (c) and 1.0 mol% Mg-doped NBT (d) using SEM. Nevertheless, the SEM images reveal small amounts of secondary phases in 1.5 mol% Mg-doped NBT (see Figure S 2 (e)). The EDX analysis revealed the secondary phases to be Mg-rich. However, the matrix shows the desired cation ratio between Na, Bi and Ti 0.5:0.5:1 within the instrument resolution. The low amount of Mg-doping content lies within the resolution limit of the used EDX analyzer (Oxford Link ISIS (Oxford Instruments Ltd., Oxfordshire, UK)). Furthermore, the $K\alpha$ energy for Na (1.04 keV) and Mg (1.25 keV) is very similar and cannot be distinguished accurately, which is responsible for the inaccuracy in the Na:Bi ratio. Table S 2 shows the measured cation ratio for the 1 mol% Mg-doped NBT composition.

Table S 2: EDX analysis of the matrix material for the 1.0 mol% Mg-doped NBT composition

EDX	Na [at%]	Bi [at%]	Ti [at%]	Mg [at%]
1.0% Mg NBT	24.84	26.10	48.49	0.53

Structural analysis:

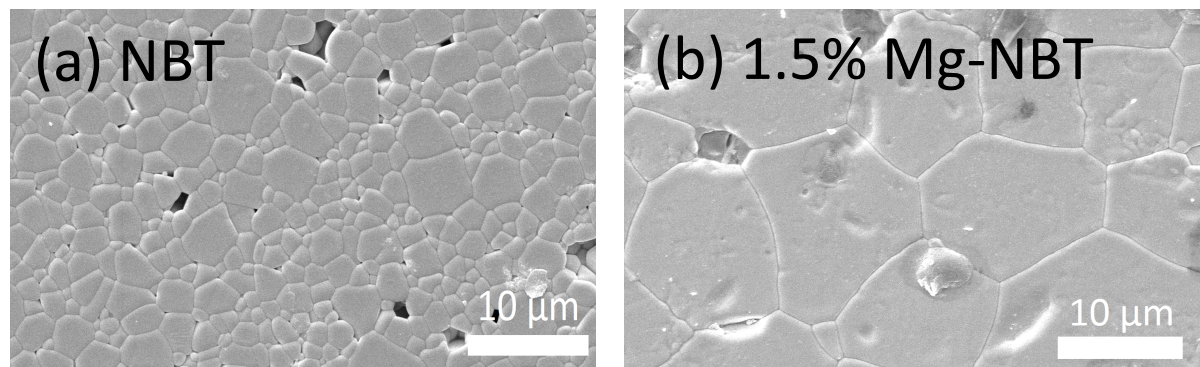


Figure S 3: SEM pictures of (a) pure NBT and (b) 1.5 mol% Mg-doped NBT in SE mode

Pure NBT (see Figure S 3 (a)) shows a dense, fine grained microstructure with an average grain size of $\sim 3 \mu\text{m}$. Mg-doped NBT, for instance, shows significantly increased grain growth at doping contents above 0.5 mol% (see 1.5% Mg-doped NBT (b) as example). The average grain size reaches a value of $\sim 14 \mu\text{m}$ at an Mg doping content of 1.5%. This phenomenon of increased grain growth is reported to be caused by an increased oxygen vacancy concentration.^{3, 4, 5}

Impedance analysis:

Different amounts of Bi-excess were used to avoid additionally formed Bi-vacancies during the processing. Figure S 4 depicts the bulk response of two different Bi-excess starting compositions. In the case of Mg-doping, the Bi-excess seems to play a minor role. Even a small excess of at least 0.1 % in the starting composition has almost the same effect as 1.0% Bi-addition regarding to the bulk response of the composition.

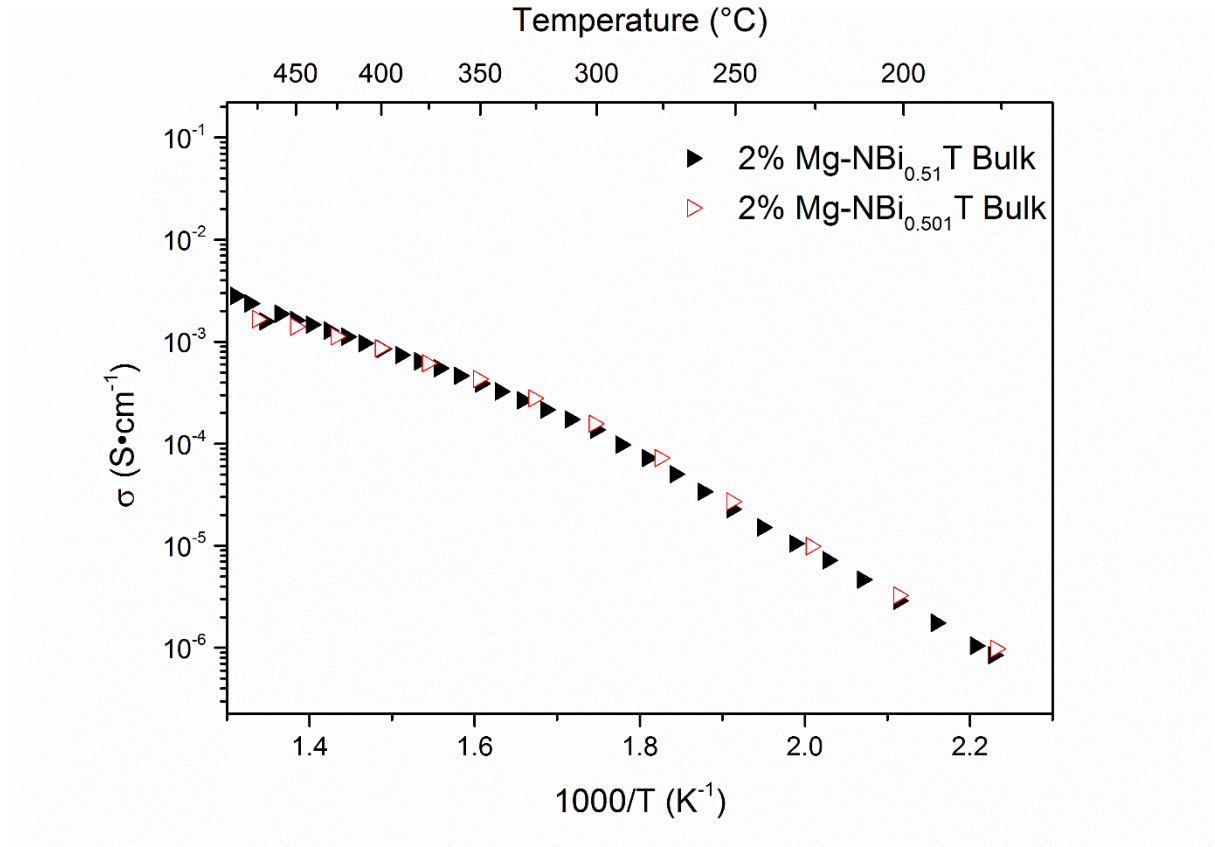


Figure S 4: Arrhenius plot of two different Bi-excess Mg-doped NBT starting compositions

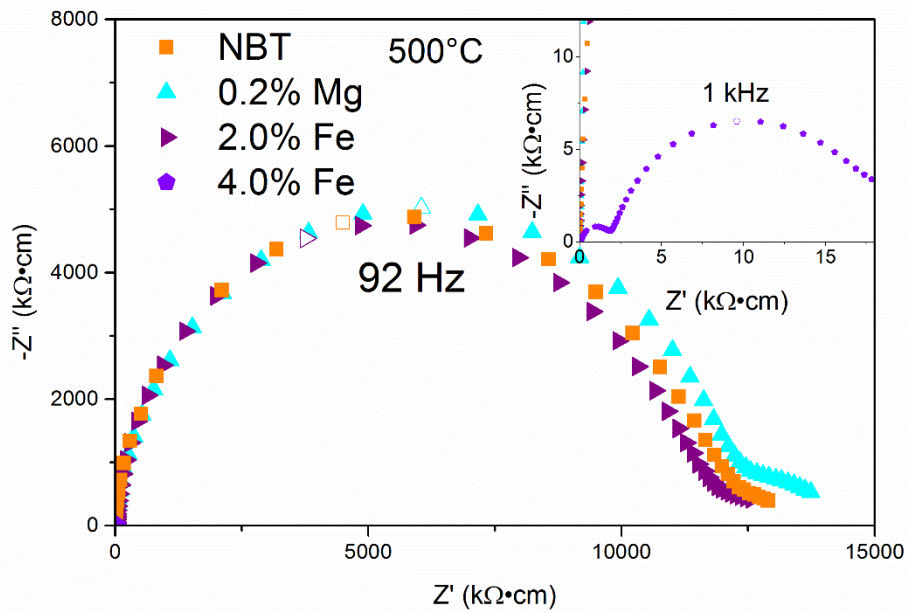


Figure S 5: Impedance plots pure NBT, 0.2 mol% Mg-doped, 2.0 mol% Fe-doped and 4.0 mol% Fe-doped NBT in Nyquist representation at 500°C. The inset shows the low resistive 4.0 mol% Fe-doped composition.

Besides pure NBT, 0.2% Mg-doped as well as 2.0% Fe-doped NBT show semiconducting behavior with single arc impedance plots (see Figure S 5). The bulk resistance R_b is approximately 12 MΩ·cm. The inset shows the impedance spectrum of 4.0% Fe-doped NBT. Two semicircles are detectable. The high frequency arc belongs to the bulk response and reaches a value of $R_b \sim 2.5$ kΩ·cm at 500°C with a peak frequency of ~ 690 kHz.

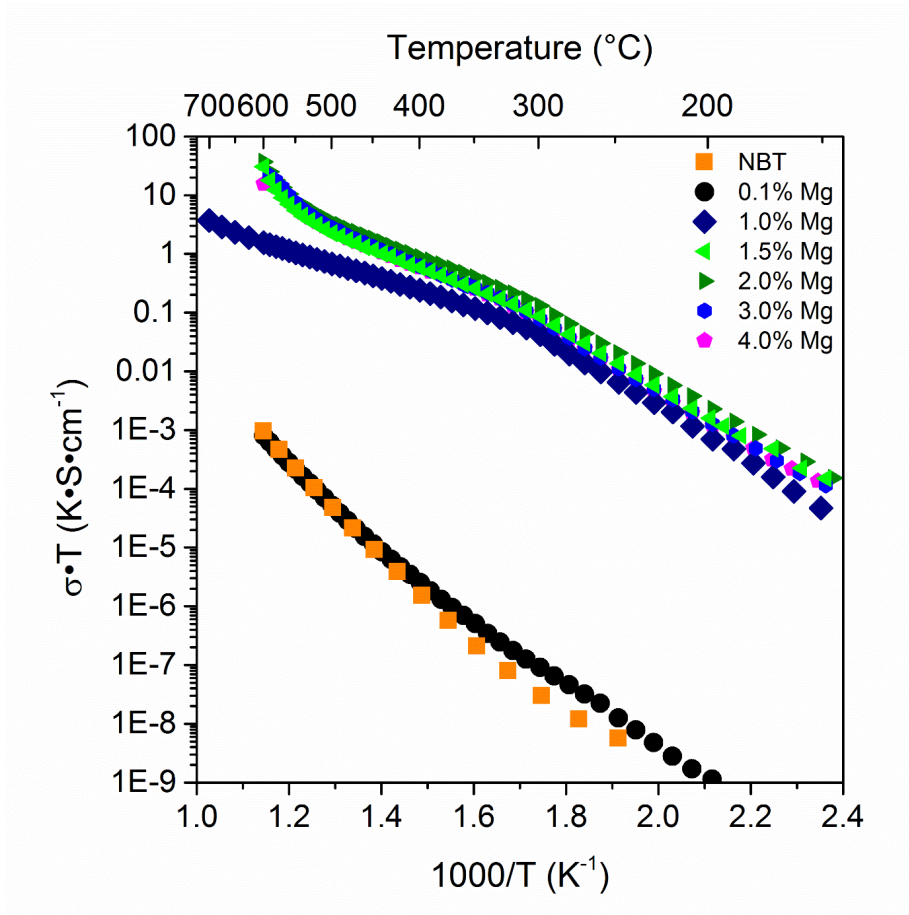


Figure S 6: Arrhenius-type plots for pure NBT as well as 0.1, 1.0, 1.5, 2.0, 3.0 and 4.0 mol% Mg-doped NBT

The Arrhenius plots for higher doped NBT compositions depicted in Figure S 6 show a saturation for Mg-doping contents higher than 1.0 mol%. Furthermore, the slope changes again at temperatures above 500°C. The bulk conductivity becomes almost independent on the acceptor doping concentration.

1. Barick BK, Mishra KK, Arora AK, Choudhary RNP, Pradhan DK. Impedance and Raman spectroscopic studies of $(\text{Na}_{0.5}\text{Bi}_{0.5})\text{TiO}_3$. *Journal of Physics D: Applied Physics* 2011, **44**(35): 355402.
2. Jones GO, Thomas PA. Investigation of the structure and phase transitions in the novel A-site substituted distorted perovskite compound $\text{Na}_{0.5}\text{Bi}_{0.5}\text{TiO}_3$. *Acta Crystallographica Section B* 2001, **B58**: 168-178.
3. Sung YS, Kim JM, Cho JH, Song TK, Kim MH, Chong HH, *et al.* Effects of Na nonstoichiometry in $(\text{Bi}_{0.5}\text{Na}_{0.5+x})\text{TiO}_3$ ceramics. *Applied Physics Letters* 2010, **96**(2): 022901.
4. Sung YS, Kim JM, Cho JH, Song TK, Kim MH, Park TG. Effects of Bi nonstoichiometry in $(\text{Bi}_{\text{sub }0.5+x}\text{Na})\text{TiO}_{\text{sub }3}$ ceramics. *Applied Physics Letters* 2011, **98**(1): 012902.
5. Seo I-T, Steiner S, Frömling T. The effect of A site non-stoichiometry on $0.94(\text{Na}_y\text{Bi}_x)\text{TiO}_3\text{-}0.06\text{BaTiO}_3$. *Journal of the European Ceramic Society* 2017, **37**(4): 1429-1436.